Inclusive Jet Production
in Two-Photon Collisions at LEP

The L3 Collaboration

Abstract

Inclusive jet production, $e^+e^- \to e^+e^-$ jet X, is studied using 560 pb^{-1} of data collected at LEP with the L3 detector at centre-of-mass energies between 189 and 209 GeV. The inclusive differential cross section is measured using a k_t jet algorithm as a function of the jet transverse momentum, p_t, in the range $3 < p_t < 50$ GeV for a pseudorapidity, η, in the range $-1 < \eta < 1$. This cross section is well represented by a power law. For high p_t, the measured cross section is significantly higher than the NLO QCD predictions, as already observed for inclusive $\pi^{\pm}$ and π^0 production.

1   Introduction

Two-photon collisions are the main source of hadron production in the high-energy regime of LEP via the process $e^+e^- \rightarrow e^+e^-\gamma^*\gamma^* \rightarrow e^+e^- hadrons$. Hadrons with high transverse momentum are produced by the direct QED process $\gamma^*\gamma^* \rightarrow q\bar{q}$ or by QCD processes originating from the partonic content of the photon. Next-to-leading order (NLO) QCD calculations are available [1, 2] for inclusive jet production in quasi-real two-photon interactions.

The L3 Collaboration published results on inclusive π^0, K_S^0 [3] and charged hadron [4] production in quasi-real two-photon collisions. The inclusive π^0 and $\pi^{\pm}$ differential cross sections, measured as a function of transverse momentum, exhibit a clear excess over NLO QCD calculations [5] for large transverse momentum. In this Letter, inclusive jet production is studied, in similar two-photon interactions, for a centre-of-mass energy of the two interacting photons, $W_{\gamma\gamma}$, greater than 5 GeV. The jets are measured in the transverse momentum range $3 < p_t < 50$ GeV and in the pseudo-rapidity interval $|\eta| < 1$. The analysis of jet production allows a comparison of the measurements to NLO QCD predictions, expected to be largely independent of fragmentation functions and hadronisation models.

2   Data and Monte Carlo

The data used for this analysis were collected by the L3 detector [6] at centre-of-mass energies $\sqrt{s} = 189 - 209$ GeV, with a luminosity weighted average value of $\sqrt{s} = 198$ GeV, and a total integrated luminosity of 560 pb^{-1}. Results on inclusive jet production at LEP for a smaller data sample at lower $\sqrt{s}$ were previously reported [7].

The process $e^+e^- \rightarrow e^+e^- hadrons$ is modelled with the PYTHIA [8] event generator with an event sample two times larger than the data. In this generator, each photon can interact as a point-like particle (direct process), as a vector meson (VDM process) or as a resolved photon (resolved process), leading to six classes of events. Since both incoming photons are assumed to be on the mass shell, PYTHIA is modified to generate the photon flux in the Equivalent Photon Approximation [9]. Predictions from the PHOJET [10] Monte Carlo program are also compared with the data. The following Monte Carlo generators are used to simulate the relevant background processes: KK2f [11] for $e^+e^- \rightarrow q\bar{q}(\gamma)$; KORALZ [12] for $e^+e^- \rightarrow \tau^+\tau^-(\gamma)$; KORALW [13] for $e^+e^- \rightarrow W^+W^-$ and DIAG36 [14] for $e^+e^- \rightarrow e^+e^-\tau^+\tau^-$. Jet hadronisation is simulated with the JETSET [8] parton shower algorithm. Events are simulated in the L3 detector using the GEANT [15] and GHEISHA [16] programs and passed through the same reconstruction program as the data. Time dependent detector inefficiencies, as monitored during each data taking period, are included in the simulations.

3   Event selection

Two-photon interaction events are collected predominantly by the track triggers [17] with a low transverse momentum threshold of about 150 MeV. The selection of $e^+e^- \rightarrow e^+e^- hadrons$ events [18] consists of:

- A multiplicity cut. To select hadronic final states, at least six objects must be detected, where an object can be a track satisfying minimal quality requirements or a calorimetric cluster of energy greater than 100 MeV.

- Energy cuts. To suppress background from beam-gas and beam-wall interactions, the total energy in the electromagnetic calorimeter is required to be greater than 500 MeV. In order to exclude e^+e^- annihilation events, the total energy deposited in the calorimeters must be less than $0.4 \sqrt{s}$.

- An anti-tag condition. Events with a cluster in the luminosity monitor, which covers the angular region $31 < \theta < 62$ mrad, with an electromagnetic shower shape and energy greater than 30 GeV are excluded.

- A mass cut. The mass of all the visible particles of the event, including clusters in the luminosity monitor, must be greater than 5 GeV. In this calculation, the pion mass is attributed to tracks and electromagnetic clusters are treated as massless. The visible mass distribution for data and Monte Carlo is shown, after all cuts, in Figure 1. A wide range of masses is accessible.

About 3 million hadronic events are selected by these criteria. The background level of this sample is less than 1% and is mainly due to the $e^+e^- \rightarrow q\bar{q}(\gamma)$, $e^+e^- \rightarrow \tau^+\tau^-$ and $e^+e^- \rightarrow e^+e^-\tau^+\tau^-$ processes.

4 Jet definition and composition

Jets are formed from good quality tracks and electromagnetic clusters. The tracks have a transverse momentum greater than 400 MeV, an absolute pseudorapidity less than 1 and a distance of closest approach to the primary vertex in the transverse plane less than 4 mm. The number of hits must be greater than 80% of the maximum number expected from the track angle. For a transverse momentum less than 20 GeV, the momentum and direction of the tracks are measured with the central tracker. For the tracks with transverse momentum above 20 GeV, the track momenta are replaced with that derived from the energy of their associated cluster in the electromagnetic and hadronic calorimeters, assuming the pion mass. Tracks associated with muon chamber hits are rejected. An electromagnetic cluster must have an energy greater than 100 MeV in at least 2 neighbouring BGO crystals and an absolute pseudorapidity less than 3.4. There should be no charged track within an angle of 200 mrad around the cluster direction and the associated energy in the hadron calorimeter must be less than 20% of the electromagnetic energy.

Jets are constructed using the k_t jet algorithm KTCLUS [19]. This algorithm uses cylindrical geometry in which the distance between two objects i, j of transverse momenta p_{ti} and p_{tj} is defined as $d_{ij} = \min(p_{ti}^2, p_{tj}^2)[(\eta_i - \eta_j)^2 + (\Phi_i - \Phi_j)^2]/D^2$ where η_i and η_j are the pseudorapidities of the objects, Φ_i and Φ_j their azimuthal angles with respect to the beam axis and D is a parameter of the algorithm which determines the size of the jet. The standard value $D = 1$ is used. A distance parameter d_k equal to p_{tk}^2 is also associated to each object. At the first iteration of the algorithm, the objects are the tracks and electromagnetic clusters defined above. At each iteration of the algorithm, the d_{ij} and d_k are ordered. If the smallest distance is a d_{ij}, the corresponding objects i and j are replaced by a new object, a "precluster", formed by adding the 4-momenta of the objects i and j. If the smallest distance is a d_k associated with a particle, this is considered as a "beam jet" particle and is removed from the list of objects. If the smallest distance is a d_k associated with a precluster, this defines a "hard jet" and is removed from the list of objects. The procedure is iterated until all objects define beam or hard jets. Only hard jets with $p_t > 3$ GeV and $|\eta| < 1$ are further considered for this analysis.

In Table 1, the data are compared to the Monte Carlo at reconstructed and generated levels for: the number of jets, the mean number of jets per event with at least one jet, the mean number of particles per jet and outside the jets. For different p_t intervals, comparisons are made of the mean number of tracks and electromagnetic clusters per jet and of transverse momentum of the leading particle divided by that of the jet. The standard deviations of these distributions are also quoted. For Monte Carlo at generator level, all particles with mean life time less than 3×10^{-10} s are allowed to decay and jets are formed from the photons, charged pions, charged and neutral kaons, protons and neutrons. Both Monte Carlo programs underestimate the number of particles inside and outside the jets. The predicted number of electromagnetic clusters is too low for all p_t. The amount of energy carried by the most energetic particle of the jet is correctly reproduced, except in the highest p_t interval. The number of particles per jet is shown in Figure 2.

Figure 3 shows the distributions of $|\eta|$ for particles, *i.e.* clusters and tracks, tracks and jets in two intervals of the jet transverse momentum, $p_t < 20$ GeV and $p_t \geq 20$ GeV. The detector acceptance for tracks, calorimetric clusters and jets is well reproduced by Monte Carlo models.

5 Differential cross section

The differential cross section for inclusive jet production as a function of p_t is measured for $W_{\gamma\gamma} \geq 5$ GeV, with a mean value of $\langle W_{\gamma\gamma} \rangle \simeq 30$ GeV, and a photon virtuality $Q^2 < 8$ GeV^2, with $\langle Q^2 \rangle \simeq 0.2$ GeV^2. This phase space is defined by Monte Carlo generator-level cuts. Results are presented in 9 p_t bins between 3 and 50 GeV.

The p_t distribution of the jets is presented in Figure 4. The total background is listed in Table 2. Events from the $e^+e^- \rightarrow e^+e^-\tau^+\tau^-$ process dominate the background at low p_t while hadronic and tau-pair annihilation events dominate it at high p_t. To measure the cross section, the background is subtracted bin-by-bin. The migration due to the p_t resolution is corrected by a one-step Bayesian unfolding [20]. The data are corrected for the selection efficiency which includes acceptance, and is calculated bin-by-bin as the ratio of the number of fully simulated jets selected in PYTHIA over the number of generated jets, as formed by the KTCLUS algorithm applied to particles at generator level. The efficiency decreases with p_t from 61% to 15%.

The level 1 trigger efficiency is obtained by comparing the number of events accepted by the independent track and calorimetric energy triggers [21]. It varies from 97% to 100%. The efficiency of higher level triggers is about 98% and is measured using prescaled events. The differential cross section and the overall efficiency, which take into account selection and trigger efficiencies, are given as a function of p_t in Table 2.

Sources of systematic uncertainties on the cross section measurements are the uncertainties on the estimation of the selection and trigger efficiencies, the limited Monte Carlo statistics, the background subtraction procedure, the selection procedure and the Monte Carlo modelling. Their contributions are shown in Table 3. The uncertainty due to the selection procedure is evaluated by repeating the analysis with different selection criteria: the multiplicity cut is moved to 5 and to 7 objects, the requirement on the number of hits of the tracks is moved to 70% of those expected, the isolation angle of clusters is moved to 100 mrad, and jets with a particle accounting for more than 90% of the jet transverse momentum are rejected. The sum in quadrature of the differences between these and the reference results is assigned as systematic uncertainty in Table 3. Varying other criteria, such as the energy cut, the minimum cluster energy or the threshold where the track energy is defined by calorimeters, gives negligible contributions. To

evaluate the uncertainty on the Monte Carlo modelling, the selection efficiency is determined using only one of the PYTHIA subprocesses: VDM-VDM, direct-direct or resolved-resolved. The systematic uncertainty is assigned as the maximum difference between these values and the reference Monte Carlo.

The differential cross sections as a function of $|\eta|$ are uniform within the experimental uncertainties for both $p_t < 20$ GeV and $p_t > 20$ GeV, albeit in the latter case these uncertainties are large.

The differential cross section $d\sigma/dp_t$ is described by a power law function $A p_t^{-B}$, as expected from the onset of hard QCD processes, with $B = 3.65 \pm 0.07$. The result of the fit is shown in Figure 5a together with a comparison to Monte Carlo predictions.

In Figure 5b the data are also compared to analytical NLO QCD predictions [2]. For this calculation, the flux of quasi-real photons is obtained using the improved Weizsäcker-Williams formula [22]. The interacting particles can be point-like photons or partons from the $\gamma \rightarrow q\bar{q}$ process, which evolve into quarks and gluons. The GRV-HO parton density functions of Reference 23 are used and all elementary $2 \rightarrow 2$ and $2 \rightarrow 3$ processes are considered. The parameter $\Lambda^{(5)}$ is set to 130 MeV. The renormalization and factorisation scales are taken to be equal: $\mu = M = E_t/2$ [1]. To assign uncertainties, the scale is varied by a factor $1/2$ or 2, which gives a change in the prediction less than 20%. The results of this calculation agree [2] with those described in Reference 24. An additional uncertainty in comparison with NLO QCD, which is not considered here, might arise from the modeling of the hadronisation process. In a similar study [25] it was evaluated to be below 10% for $p_t > 10$ GeV and decreasing with increasing p_t. The agreement with the data is poor in the high-p_t range, as previously observed in the case of inclusive π^0 [3] and $\pi^\pm$ [4] production in similar two-photon reactions. In Figure 6, the data are divided in two $W_{\gamma\gamma}$ ranges, $W_{\gamma\gamma} > 50$ GeV and $W_{\gamma\gamma} \geq 50$ GeV and compared to the analytical NLO QCD predictions [2]. For $W_{\gamma\gamma} \geq 50$ GeV there is a clear discontinuity in the slope near $p_t = 25$ GeV, due to the direct contribution. At high p_t, the disagreement between data and theoretical calculations is still present.

References

[1] S. Frixione, Nucl. Phys. **B 507** (1997) 295 ;
    S. Frixione and G. Ridolfi, Nucl. Phys. **B 507** (1997) 315.

[2] L. Bertora, Nucl. Phys. **B 126** (2004) 134 (Proc. Syppl.)
    S. Frixione and L. Bertora, private communication.
    We thank the authors for providing us with the NLO QCD calculations and for useful discussions.

[3] L3 Collaboration, P. Achard *et al.*, Phys. Lett. **B 524** (2002) 44.

[4] L3 Collaboration, P. Achard *et al.*, Phys. Lett. **B 554** (2003) 105.

[5] J. Binnewies, B. A. Kniehl and G. Kramer, Phys. Rev. **D 53** (1996) 6110.

[6] L3 Collaboration, B. Adeva *et al.*, Nucl. Instr. Meth. **A 289** (1990) 35;
    M. Chemarin *et al.*, Nucl. Instr. Meth. **A 349** (1994) 345;
    M. Acciarri *et al.*, Nucl. Instr. Meth. **A 351** (1994) 300;
    G. Basti *et al.*, Nucl. Instr. Meth. **A 374** (1996) 293;

I. C. Brock *et al.*, Nucl. Instr. Meth. **A 381** (1996) 236;
A. Adam *et al.*, Nucl. Instr. Meth. **A 383** (1996) 342.

[7] OPAL Collaboration, K. Ackerstaff *et al.*, Z. Phys. **C 73** (1997) 433.

[8] PYTHIA version 5.722 and JETSET version 7.409 are used with default options;
T. Sjöstrand, Comp. Phys. Comm. **82** (1994) 74.

[9] V. M. Budnev *et al.*. Phys. Rep. **15** (1974) 181.

[10] PHOJET version 1.05c is used with default options;
R. Engel, Z. Phys. **C 66** (1995) 203;
R. Engel and J. Ranft, Phys. Rev. **D 54** (1996) 4246.

[11] KK2f version 4.12 is used;
S. Jadach, B. F. L. Ward and Z. Wąs, Comp. Phys. Comm. **130** (2000) 260.

[12] KORALZ version 4.04 is used;
S. Jadach, B. F. L. Ward and Z. Wąs, Comp. Phys. Comm. **79** (1994) 503.

[13] KORALW version 1.33 is used;
M. Skrzypek *et al.*, Comp. Phys. Comm. **94** (1996) 216.

[14] DIAG36 Monte Carlo;
F. A. Berends, P. H. Daverfeldt and R. Kleiss, Nucl. Phys. **B 253** (1985) 441.

[15] GEANT version 3.15 is used;
R. Brun *et al.*, preprint CERN DD/EE/84-1 (1984), revised 1987.

[16] H. Fesefeldt, RWTH Aachen report PITHA 85/2 (1985).

[17] P. Béné *et al.*, Nucl. Instr. Meth. **A 306** (1991) 150;
D. Haas *et al.*, Nucl. Instr. Meth. **A 420** (1999) 101.

[18] L3 Collaboration, M. Acciarri *et al.*, Phys. Lett. **B 519** (2001) 33.

[19] S. Catani *et al.*, Nucl. Phys. **B 406** (1993) 187;
S.D. Ellis and D.E. Soper, Phys. Rev. **D 48** (1993) 3160;
M. Seymour, http://hepwww.rl.ac.uk/theory/seymour/ktclus/

[20] G. D'Agostini, Nucl. Instr. Meth. **A 362** (1995) 487.

[21] R. Bizzarri *et al.*, Nucl. Instr. Meth. **A 283** (1989) 799.

[22] S. Frixione *et al.*, Phys. Lett. **B 319** (1993) 339.

[23] M. Gluck, E. Reya and A. Vogt, Phys. Rev. **D 45** (1992) 3986;
M. Gluck, E. Reya and A. Vogt, Phys. Rev. **D 46** (1992) 1973.

[24] T. Kleinwort and G. Kramer Nucl. Phys. **B 477** (1996) 3;
M. Klasen, T. Kleinwort and G. Kramer Eur. Phys. J. **C 1** (1998) 1.

[25] OPAL Collaboration, G. Abbiendi *et al.*., Eur. Phys. J. **C 31** (2003) 307.

Author List

The L3 Collaboration:

P.Achard[20] O.Adriani[17] M.Aguilar-Benitez[24] J.Alcaraz[24] G.Alemanni[22] J.Allaby[18] A.Aloisio[28] M.G.Alviggi[28]
H.Anderhub[46] V.P.Andreev[6,33] F.Anselmo[8] A.Arefiev[27] T.Azemoon[3] T.Aziz[9] P.Bagnaia[38] A.Bajo[24] G.Baksay[25]
L.Baksay[25] S.V.Baldew[2] S.Banerjee[9] Sw.Banerjee[4] A.Barczyk[46,44] R.Barillère[18] P.Bartalini[22] M.Basile[8]
N.Batalova[43] R.Battiston[32] A.Bay[22] F.Becattini[17] U.Becker[13] F.Behner[46] L.Bellucci[17] R.Berbeco[3] J.Berdugo[24]
P.Berges[13] B.Bertucci[32] B.L.Betev[46] M.Biasini[32] M.Biglietti[28] A.Biland[46] J.J.Blaising[4] S.C.Blyth[34]
G.J.Bobbink[2] A.Böhm[1] L.Boldizsar[12] B.Borgia[38] S.Bottai[17] D.Bourilkov[46] M.Bourquin[20] S.Braccini[20]
J.G.Branson[40] F.Brochu[4] J.D.Burger[13] W.J.Burger[32] X.D.Cai[13] M.Capell[13] G.Cara Romeo[8] G.Carlino[28]
A.Cartacci[17] J.Casaus[24] F.Cavallari[38] N.Cavallo[35] C.Cecchi[32] M.Cerrada[24] M.Chamizo[20] Y.H.Chang[48]
M.Chemarin[23] A.Chen[48] G.Chen[7] G.M.Chen[7] H.F.Chen[21] H.S.Chen[7] G.Chiefari[28] L.Cifarelli[39] F.Cindolo[8]
I.Clare[13] R.Clare[37] G.Coignet[4] N.Colino[24] S.Costantini[38] B.de la Cruz[24] S.Cucciarelli[32] J.A.van Dalen[30]
R.de Asmundis[28] P.Déglon[20] J.Debreczeni[12] A.Degré[4] K.Dehmelt[25] K.Deiters[44] D.della Volpe[28] E.Delmeire[20]
P.Denes[36] F.DeNotaristefani[38] A.De Salvo[46] M.Diemoz[38] M.Dierckxsens[2] C.Dionisi[38] M.Dittmar[46] A.Doria[28]
M.T.Dova[10,♯] D.Duchesneau[4] M.Duda[1] B.Echenard[20] A.Eline[18] A.El Hage[1] H.El Mamouni[23] A.Engler[34]
F.J.Eppling[13] P.Extermann[20] M.A.Falagan[24] S.Falciano[38] A.Favara[31] J.Fay[23] O.Fedin[33] M.Felcini[46] T.Ferguson[34]
H.Fesefeldt[1] E.Fiandrini[32] J.H.Field[20] F.Filthaut[30] P.H.Fisher[13] W.Fisher[36] I.Fisk[40] G.Forconi[13]
K.Freudenreich[46] C.Furetta[26] Yu.Galaktionov[27,13] S.N.Ganguli[9] P.Garcia-Abia[24] M.Gataullin[31] S.Gentile[38]
S.Giagu[38] Z.F.Gong[21] G.Grenier[23] O.Grimm[46] M.W.Gruenewald[16] M.Guida[39] R.van Gulik[2] V.K.Gupta[36]
A.Gurtu[9] L.J.Gutay[43] D.Haas[5] D.Hatzifotiadou[8] T.Hebbeker[1] A.Hervé[18] J.Hirschfelder[34] H.Hofer[46]
M.Hohlmann[25] G.Holzner[46] S.R.Hou[48] Y.Hu[30] B.N.Jin[7] L.W.Jones[3] P.de Jong[2] I.Josa-Mutuberría[24] D.Käfer[1]
M.Kaur[14] M.N.Kienzle-Focacci[20] J.K.Kim[42] J.Kirkby[18] W.Kittel[30] A.Klimentov[13,27] A.C.König[30] M.Kopal[43]
V.Koutsenko[13,27] M.Kräber[46] R.W.Kraemer[34] A.Krüger[45] A.Kunin[13] P.Ladron de Guevara[24] I.Laktineh[23]
G.Landi[17] M.Lebeau[18] A.Lebedev[13] P.Lebrun[23] P.Lecomte[46] P.Lecoq[18] P.Le Coultre[46] J.M.Le Goff[18] R.Leiste[45]
M.Levtchenko[26] P.Levtchenko[33] C.Li[21] S.Likhoded[45] C.H.Lin[48] W.T.Lin[48] F.L.Linde[2] L.Lista[28] Z.A.Liu[7]
W.Lohmann[45] E.Longo[38] Y.S.Lu[7] C.Luci[38] L.Luminari[38] W.Lustermann[46] W.G.Ma[21] L.Malgeri[20] A.Malinin[27]
C.Maña[24] J.Mans[36] J.P.Martin[23] F.Marzano[38] K.Mazumdar[9] R.R.McNeil[6] S.Mele[18,28] L.Merola[28] M.Meschini[17]
W.J.Metzger[30] A.Mihul[11] H.Milcent[18] G.Mirabelli[38] J.Mnich[1] G.B.Mohanty[9] G.S.Muanza[23] A.J.M.Muijs[2]
B.Musicar[40] M.Musy[38] S.Nagy[15] S.Natale[20] M.Napolitano[28] F.Nessi-Tedaldi[46] H.Newman[31] A.Nisati[38]
T.Novak[30] H.Nowak[45] R.Ofierzynski[46] G.Organtini[38] I.Pal[43] C.Palomares[24] P.Paolucci[28] R.Paramatti[38]
G.Passaleva[17] S.Patricelli[28] T.Paul[10] M.Pauluzzi[32] C.Paus[13] F.Pauss[46] M.Pedace[38] S.Pensotti[26] D.Perret-Gallix[4]
B.Petersen[30] D.Piccolo[28] F.Pierella[8] M.Pioppi[32] P.A.Piroué[36] E.Pistolesi[26] V.Plyaskin[27] M.Pohl[20] V.Pojidaev[17]
J.Pothier[18] D.Prokofiev[33] J.Quartieri[39] G.Rahal-Callot[46] M.A.Rahaman[9] P.Raics[15] N.Raja[9] R.Ramelli[46]
P.G.Rancoita[26] R.Ranieri[17] A.Raspereza[45] P.Razis[29] D.Ren[46] M.Rescigno[38] S.Reucroft[10] S.Riemann[45] K.Riles[3]
B.P.Roe[3] L.Romero[24] A.Rosca[45] C.Rosenbleck[1] S.Rosier-Lees[4] S.Roth[1] J.A.Rubio[18] G.Ruggiero[17]
H.Rykaczewski[46] A.Sakharov[46] S.Saremi[6] S.Sarkar[38] J.Salicio[18] E.Sanchez[24] C.Schäfer[18] V.Schegelsky[33]
H.Schopper[47] D.J.Schotanus[30] C.Sciacca[28] L.Servoli[32] S.Shevchenko[31] N.Shivarov[41] V.Shoutko[13] E.Shumilov[27]
A.Shvorob[31] D.Son[42] C.Souga[23] P.Spillantini[17] M.Steuer[13] D.P.Stickland[36] B.Stoyanov[41] A.Straessner[20]
K.Sudhakar[9] G.Sultanov[41] L.Z.Sun[21] S.Sushkov[1] H.Suter[46] J.D.Swain[10] Z.Szillasi[25,¶] X.W.Tang[7] P.Tarjan[15]
L.Tauscher[5] L.Taylor[10] B.Tellili[23] D.Teyssier[23] C.Timmermans[30] Samuel C.C.Ting[13] S.M.Ting[13] S.C.Tonwar[9]
J.Tóth[12] C.Tully[36] K.L.Tung[7] J.Ulbricht[46] E.Valente[38] R.T.Van de Walle[30] R.Vasquez[43] V.Veszpremi[25]
G.Vesztergombi[12] I.Vetlitsky[27] D.Vicinanza[39] G.Viertel[46] S.Villa[37] M.Vivargent[4] S.Vlachos[5] I.Vodopianov[25]
H.Vogel[34] H.Vogt[45] I.Vorobiev[34,27] A.A.Vorobyov[33] M.Wadhwa[5] Q.Wang[30] X.L.Wang[21] Z.M.Wang[21] M.Weber[1]
P.Wienemann[1] H.Wilkens[30] S.Wynhoff[36] L.Xia[31] Z.Z.Xu[21] J.Yamamoto[3] B.Z.Yang[21] C.G.Yang[7] H.J.Yang[3]
M.Yang[7] S.C.Yeh[49] An.Zalite[33] Yu.Zalite[33] Z.P.Zhang[21] J.Zhao[21] G.Y.Zhu[7] R.Y.Zhu[31] H.L.Zhuang[7]
A.Zichichi[8,18,19] B.Zimmermann[46] M.Zöller[1]

1 III. Physikalisches Institut, RWTH, D-52056 Aachen, Germany[§]
2 National Institute for High Energy Physics, NIKHEF, and University of Amsterdam, NL-1009 DB Amsterdam, The Netherlands
3 University of Michigan, Ann Arbor, MI 48109, USA
4 Laboratoire d'Annecy-le-Vieux de Physique des Particules, LAPP,IN2P3-CNRS, BP 110, F-74941 Annecy-le-Vieux CEDEX, France
5 Institute of Physics, University of Basel, CH-4056 Basel, Switzerland
6 Louisiana State University, Baton Rouge, LA 70803, USA
7 Institute of High Energy Physics, IHEP, 100039 Beijing, China[△]
8 University of Bologna and INFN-Sezione di Bologna, I-40126 Bologna, Italy
9 Tata Institute of Fundamental Research, Mumbai (Bombay) 400 005, India
10 Northeastern University, Boston, MA 02115, USA
11 Institute of Atomic Physics and University of Bucharest, R-76900 Bucharest, Romania
12 Central Research Institute for Physics of the Hungarian Academy of Sciences, H-1525 Budapest 114, Hungary[‡]
13 Massachusetts Institute of Technology, Cambridge, MA 02139, USA
14 Panjab University, Chandigarh 160 014, India.
15 KLTE-ATOMKI, H-4010 Debrecen, Hungary[¶]
16 Department of Experimental Physics, University College Dublin, Belfield, Dublin 4, Ireland
17 INFN Sezione di Firenze and University of Florence, I-50125 Florence, Italy
18 European Laboratory for Particle Physics, CERN, CH-1211 Geneva 23, Switzerland
19 World Laboratory, FBLJA Project, CH-1211 Geneva 23, Switzerland
20 University of Geneva, CH-1211 Geneva 4, Switzerland
21 Chinese University of Science and Technology, USTC, Hefei, Anhui 230 029, China[△]
22 University of Lausanne, CH-1015 Lausanne, Switzerland
23 Institut de Physique Nucléaire de Lyon, IN2P3-CNRS,Université Claude Bernard, F-69622 Villeurbanne, France
24 Centro de Investigaciones Energéticas, Medioambientales y Tecnológicas, CIEMAT, E-28040 Madrid, Spain[♭]
25 Florida Institute of Technology, Melbourne, FL 32901, USA
26 INFN-Sezione di Milano, I-20133 Milan, Italy
27 Institute of Theoretical and Experimental Physics, ITEP, Moscow, Russia
28 INFN-Sezione di Napoli and University of Naples, I-80125 Naples, Italy
29 Department of Physics, University of Cyprus, Nicosia, Cyprus
30 University of Nijmegen and NIKHEF, NL-6525 ED Nijmegen, The Netherlands
31 California Institute of Technology, Pasadena, CA 91125, USA
32 INFN-Sezione di Perugia and Università Degli Studi di Perugia, I-06100 Perugia, Italy
33 Nuclear Physics Institute, St. Petersburg, Russia
34 Carnegie Mellon University, Pittsburgh, PA 15213, USA
35 INFN-Sezione di Napoli and University of Potenza, I-85100 Potenza, Italy
36 Princeton University, Princeton, NJ 08544, USA
37 University of Californa, Riverside, CA 92521, USA
38 INFN-Sezione di Roma and University of Rome, "La Sapienza", I-00185 Rome, Italy
39 University and INFN, Salerno, I-84100 Salerno, Italy
40 University of California, San Diego, CA 92093, USA
41 Bulgarian Academy of Sciences, Central Lab. of Mechatronics and Instrumentation, BU-1113 Sofia, Bulgaria
42 The Center for High Energy Physics, Kyungpook National University, 702-701 Taegu, Republic of Korea
43 Purdue University, West Lafayette, IN 47907, USA
44 Paul Scherrer Institut, PSI, CH-5232 Villigen, Switzerland
45 DESY, D-15738 Zeuthen, Germany
46 Eidgenössische Technische Hochschule, ETH Zürich, CH-8093 Zürich, Switzerland
47 University of Hamburg, D-22761 Hamburg, Germany
48 National Central University, Chung-Li, Taiwan, China
49 Department of Physics, National Tsing Hua University, Taiwan, China

Variable	Data	PYTHIA		PHOJET	
		Reconstructed	Generated	Reconstructed	Generated
Total number of jets	68792	107140	188302	65781	105633
Number of jets / event	1.2 ± 0.1 (0.5)	1.4 (0.7)	1.3 (0.7)	1.2 (0.4)	1.1 (0.5)
N(particles) / jet	6.1 ± 0.1 (2.5)	5.4 (2.3)	5.3 (2.4)	5.7 (2.4)	6.1 (2.4)
N(particles) outside jets	14.4 ± 0.1 (8.4)	10.0 (7.0)	13.6 (9.3)	12.4 (7.3)	18.4 (8.8)
N(tracks) / jet $\quad 3 < p_t < 5$ GeV	2.2 ± 0.1 (1.3)	2.3 (1.3)		2.4 (1.3)	
$\quad\quad 5 < p_t < 10$ GeV	2.4 ± 0.1 (1.3)	2.6 (1.3)		2.8 (1.4)	
$\quad\quad 10 < p_t < 25$ GeV	2.5 ± 0.1 (1.6)	2.9 (1.3)		3.0 (1.6)	
$\quad\quad 25 < p_t < 45$ GeV	2.7 ± 0.2 (1.7)	3.3 (1.6)		−	
N(clusters) / jet $\quad 3 < p_t < 5$ GeV	3.7 ± 0.1 (2.4)	2.0 (2.0)		3.1 (2.2)	
$\quad\quad 5 < p_t < 10$ GeV	3.9 ± 0.1 (2.6)	1.8 (1.9)		3.3 (2.4)	
$\quad\quad 10 < p_t < 25$ GeV	3.9 ± 0.1 (3.0)	1.6 (1.8)		3.3 (2.5)	
$\quad\quad 25 < p_t < 45$ GeV	3.8 ± 0.3 (3.0)	1.4 (1.7)		−	
p_t(leading) / p_t $\quad 3 < p_t < 5$ GeV	0.50 ± 0.01 (0.18)	0.53 (0.18)	0.50 (0.18)	0.51 (0.18)	0.46 (0.17)
$\quad\quad 5 < p_t < 10$ GeV	0.54 ± 0.01 (0.20)	0.55 (0.19)	0.50 (0.20)	0.52 (0.19)	0.43 (0.17)
$\quad\quad 10 < p_t < 25$ GeV	0.63 ± 0.01 (0.23)	0.60 (0.20)	0.48 (0.22)	0.60 (0.24)	0.39 (0.19)
$\quad\quad 25 < p_t < 45$ GeV	0.69 ± 0.03 (0.23)	0.56 (0.14)	0.47 (0.25)	−	−

Table 1: Mean value and standard deviation (in brackets) of multiplicities and p_t fractions for the jets in data and Monte Carlo events, at generator level as well as after reconstruction. The uncertainties on the mean values are quoted for the data. For Monte Carlo, they are always lower than the precision of the last digit.

p_t [GeV]	$\langle p_t \rangle$ [GeV]	Background [%]	Reconstruction efficiency [%]	Trigger efficiency [%]	$d\sigma/dp_t$ [pb/GeV]	
3−4	3.4	4.6 ± 0.1	60.8 ± 0.2	95.8 ± 0.3	$(13 \pm 1 \pm 1)$	$\times 10^{1}$
4−5	4.4	5.6 ± 0.1	57.2 ± 0.3	95.9 ± 0.5	$(40 \pm 1 \pm 3)$	
5−7.5	5.9	7.8 ± 0.1	53.2 ± 0.3	96.2 ± 0.5	$(11 \pm 1 \pm 1)$	
7.5−10	8.5	11.1 ± 0.1	48.9 ± 0.5	96.6 ± 1.0	$(30 \pm 1 \pm 2)$	$\times 10^{-1}$
10−15	11.9	14.0 ± 0.2	44.9 ± 0.6	96.8 ± 1.4	$(88 \pm 3 \pm 7)$	$\times 10^{-2}$
15−20	17.1	16.0 ± 0.4	39.2 ± 0.9	96.9 ± 2.0	$(30 \pm 2 \pm 3)$	$\times 10^{-2}$
20−30	24.0	18.6 ± 0.8	31.6 ± 0.8	97.3 ± 2.1	$(90 \pm 7 \pm 8)$	$\times 10^{-3}$
30−40	34.1	18.9 ± 1.5	20.5 ± 1.3	97.3 ± 2.5	$(31 \pm 5 \pm 2)$	$\times 10^{-3}$
40−50	44.7	19.6 ± 1.6	15.2 ± 1.9	98.5 ± 2.8	$(11 \pm 3 \pm 2)$	$\times 10^{-3}$

Table 2: Background level, reconstruction efficiency, trigger efficiency and differential cross section as a function of p_t for $|\eta| < 1$ and $W_{\gamma\gamma} > 5$ GeV. The first uncertainty is statistical and the second systematic. The average value of p_t for each bin, $\langle p_t \rangle$, is also given.

p_t [GeV]	Trigger efficiency [%]	Monte Carlo statistics [%]	Background subtraction [%]	Selection procedure [%]	Monte Carlo modelling [%]
3−4	0.3	0.3	< 0.1	8.4	0.3
4−5	0.5	0.5	0.2	7.0	1.3
5−7.5	0.5	0.5	0.3	6.6	1.5
7.5−10	1.0	1.0	0.6	4.8	2.4
10−15	1.4	1.3	0.9	7.0	2.6
15−20	2.1	2.4	1.7	8.0	3.3
20−30	2.2	2.6	2.7	6.0	4.8
30−40	2.6	6.4	5.2	< 0.1	6.2
40−50	2.8	12.4	9.6	< 0.1	12.4

Table 3: Systematic uncertainties on the inclusive jet cross section as a function of p_t.
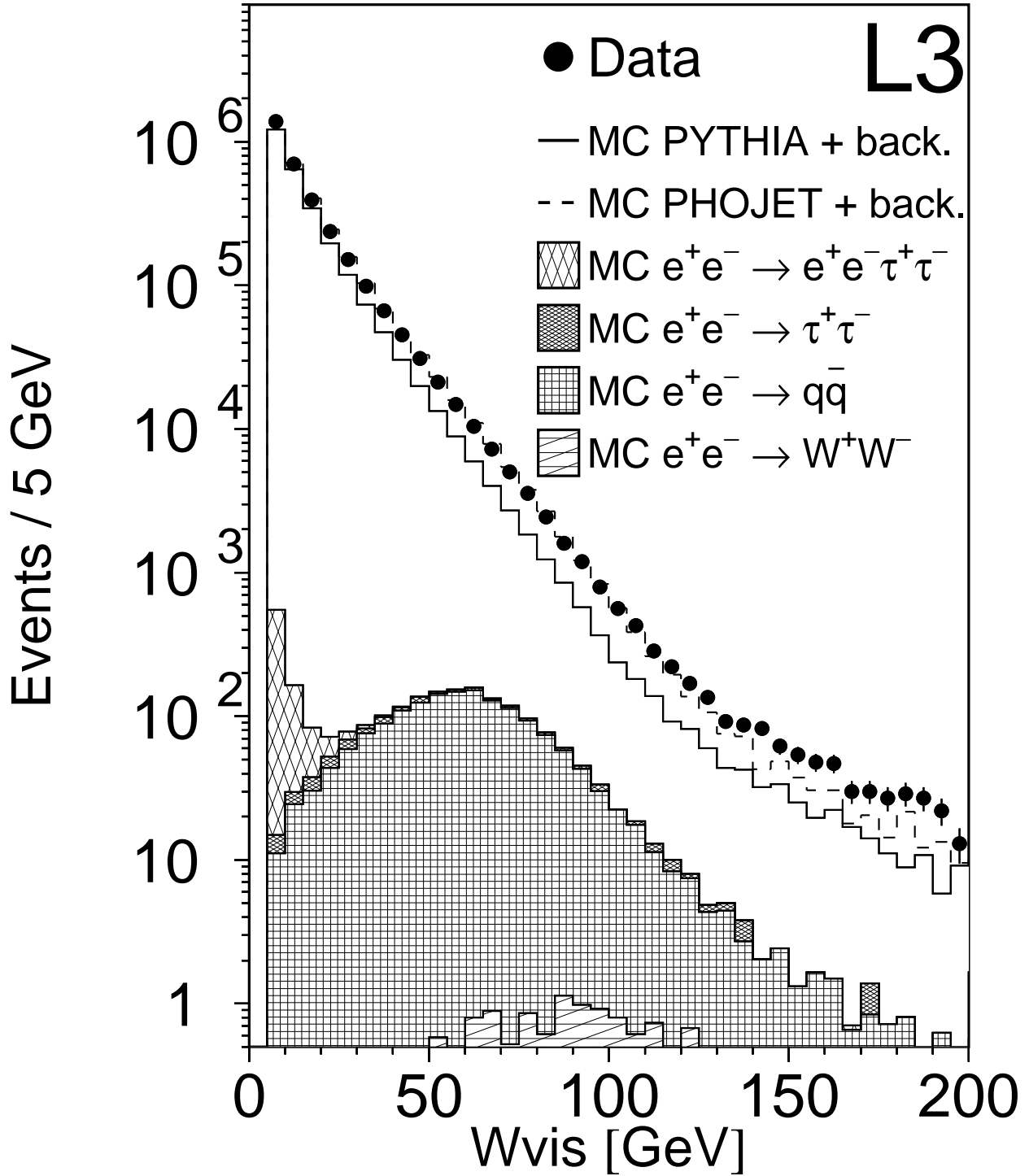
Figure 1: Distribution of the visible mass for selected events. The Monte Carlo distributions are normalised to the luminosity of the data. Various contributions to the background (back.) are shown as cumulative histograms.
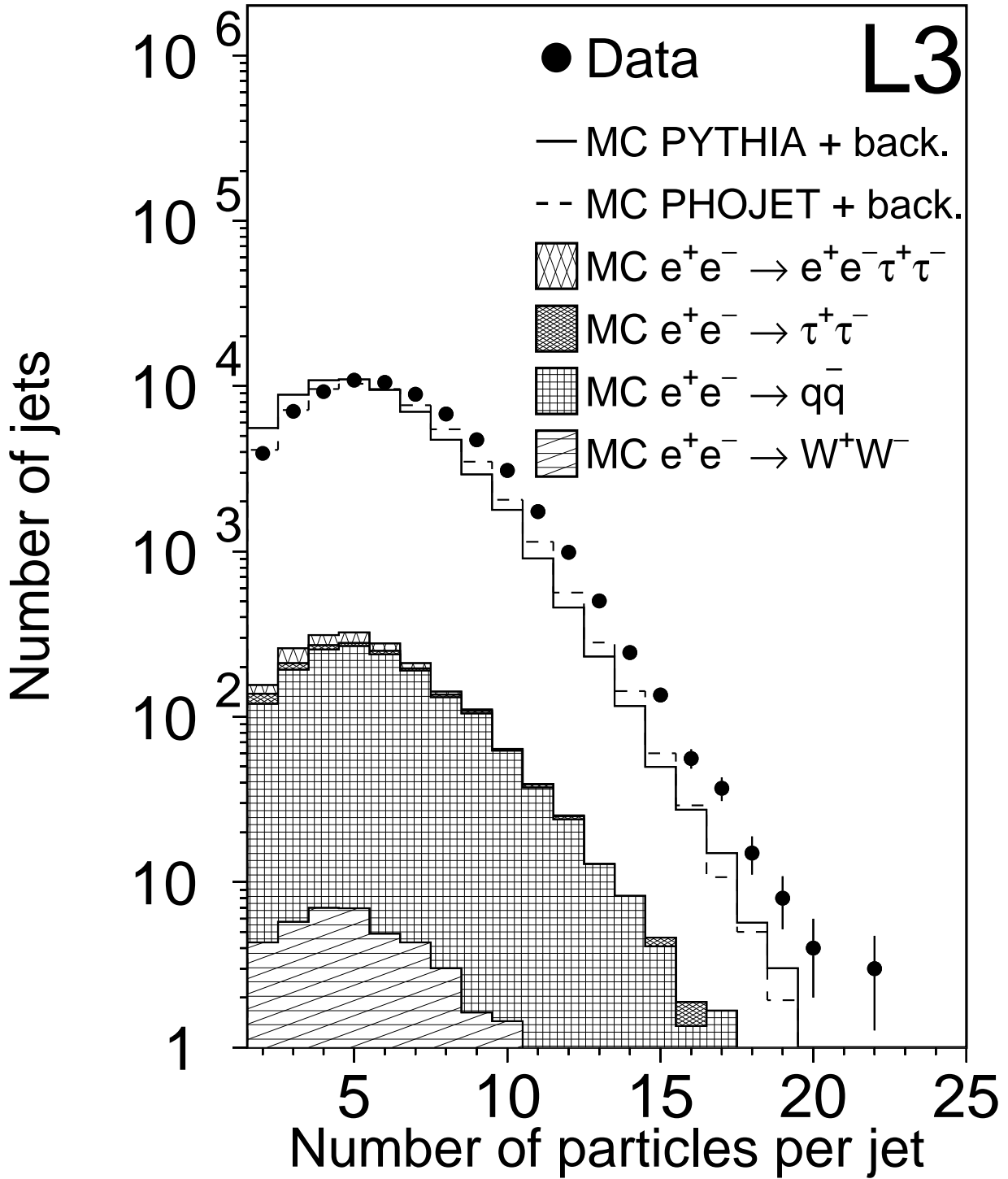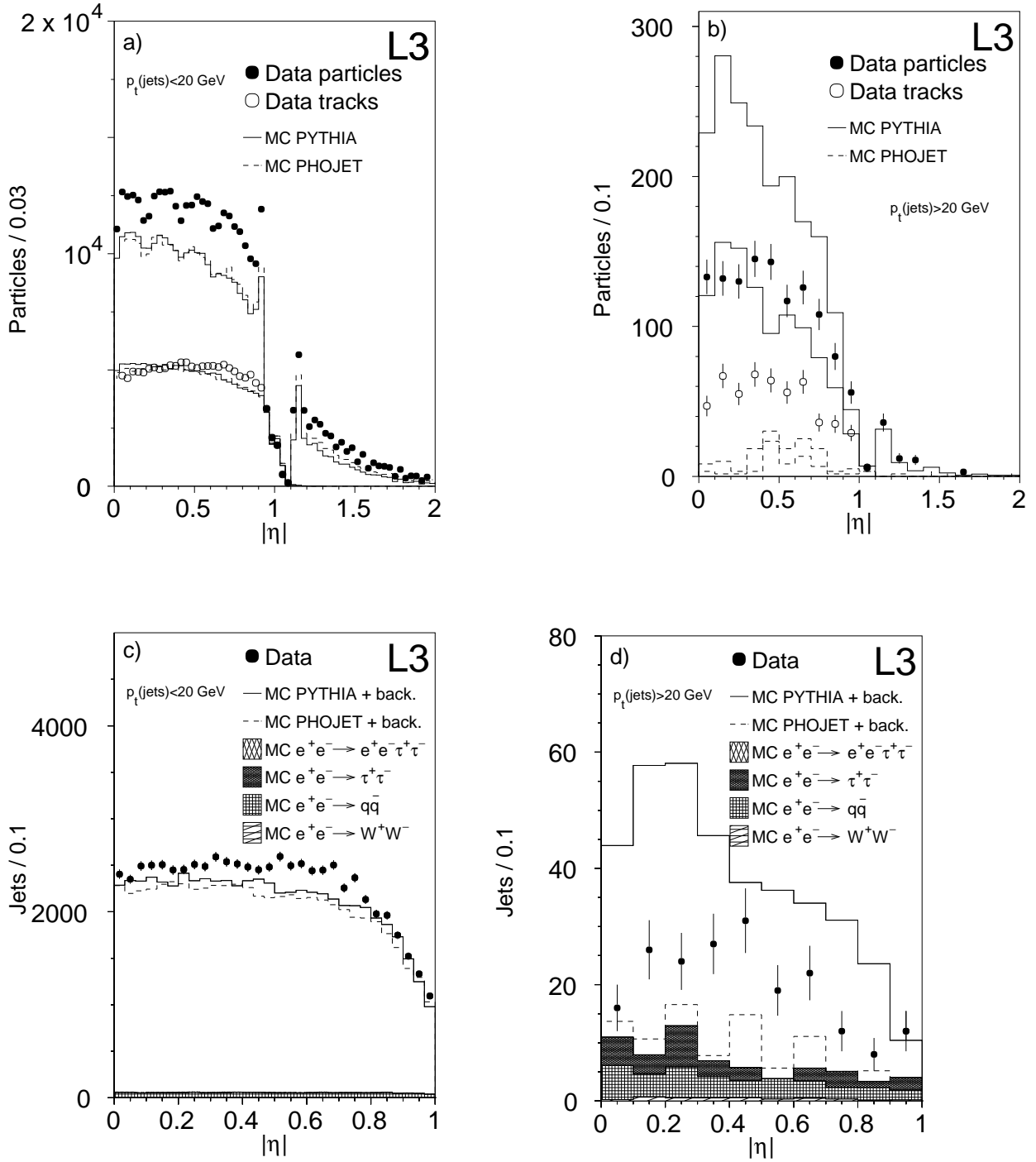
Figure 2: Distribution of the number of particles per jet for jets with $p_t > 3$ GeV and $|\eta| < 1$. The Monte Carlo distributions are normalised to the luminosity of the data. Various contributions to the background (back.) are shown as cumulative histograms.

Figure 3: Distributions of the pseudo rapidity $|\eta|$ for a) and b) particles and tracks used to form jets with $p_t < 20$ GeV and $p_t \geq 20$ GeV, respectively. "Particles" include both calorimetric clusters and tracks. c) and d) distributions of $|\eta|$ for reconstructed jets with $p_t < 20$ GeV and $p_t \geq 20$ GeV, respectively. The Monte Carlo distributions are normalised to the luminosity of the data. In a) and b) the higher Monte Carlo lines refer to particles and the lower ones to tracks. Various contributions to the background are shown as cumulative histograms in c) and d).
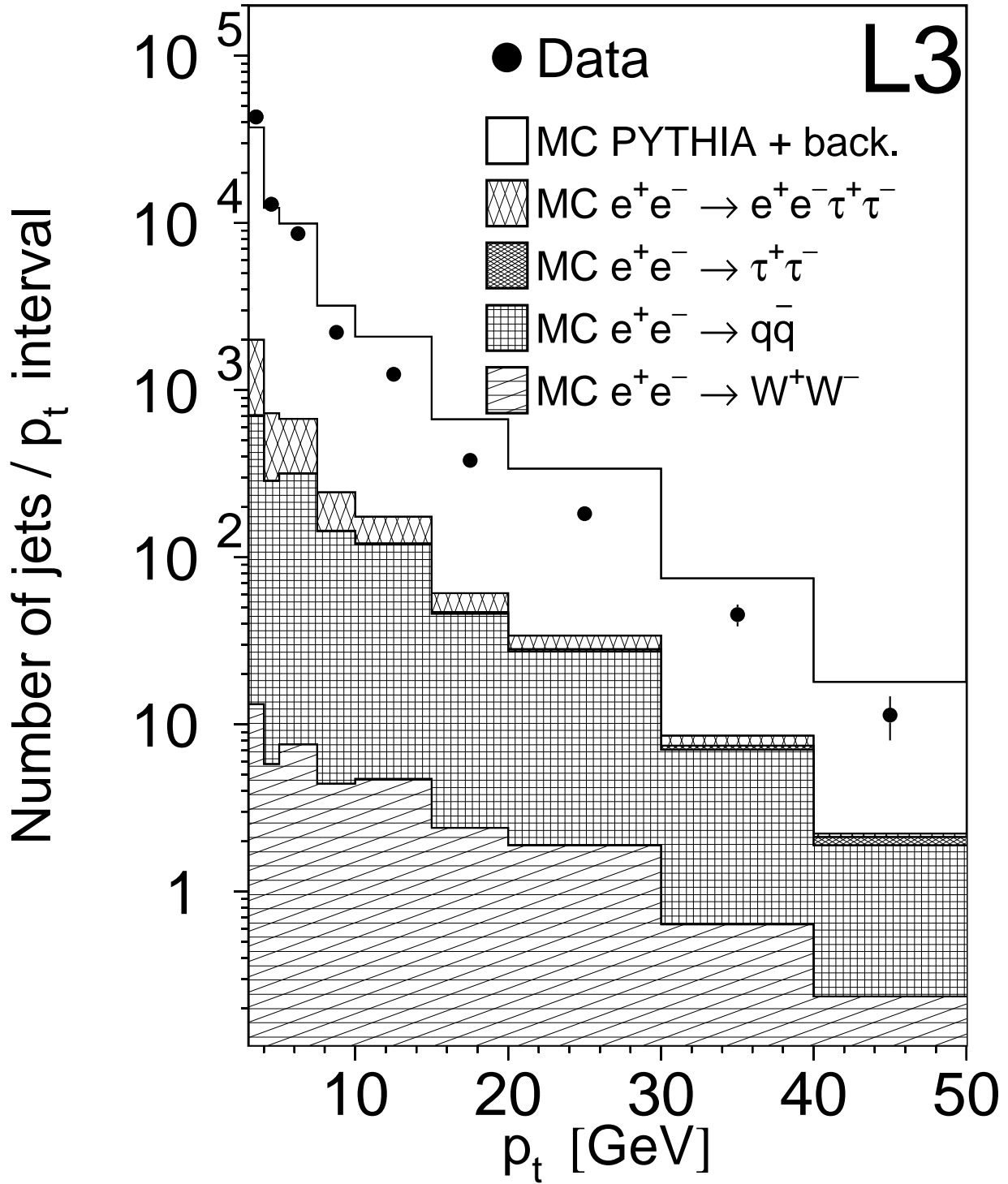
13

Figure 4: Distribution of the number of jets with $|\eta| < 1$ as a function of p_t. The Monte Carlo distributions are normalised to the luminosity of the data. Various contributions to the background (back.) are shown as cumulative histograms.
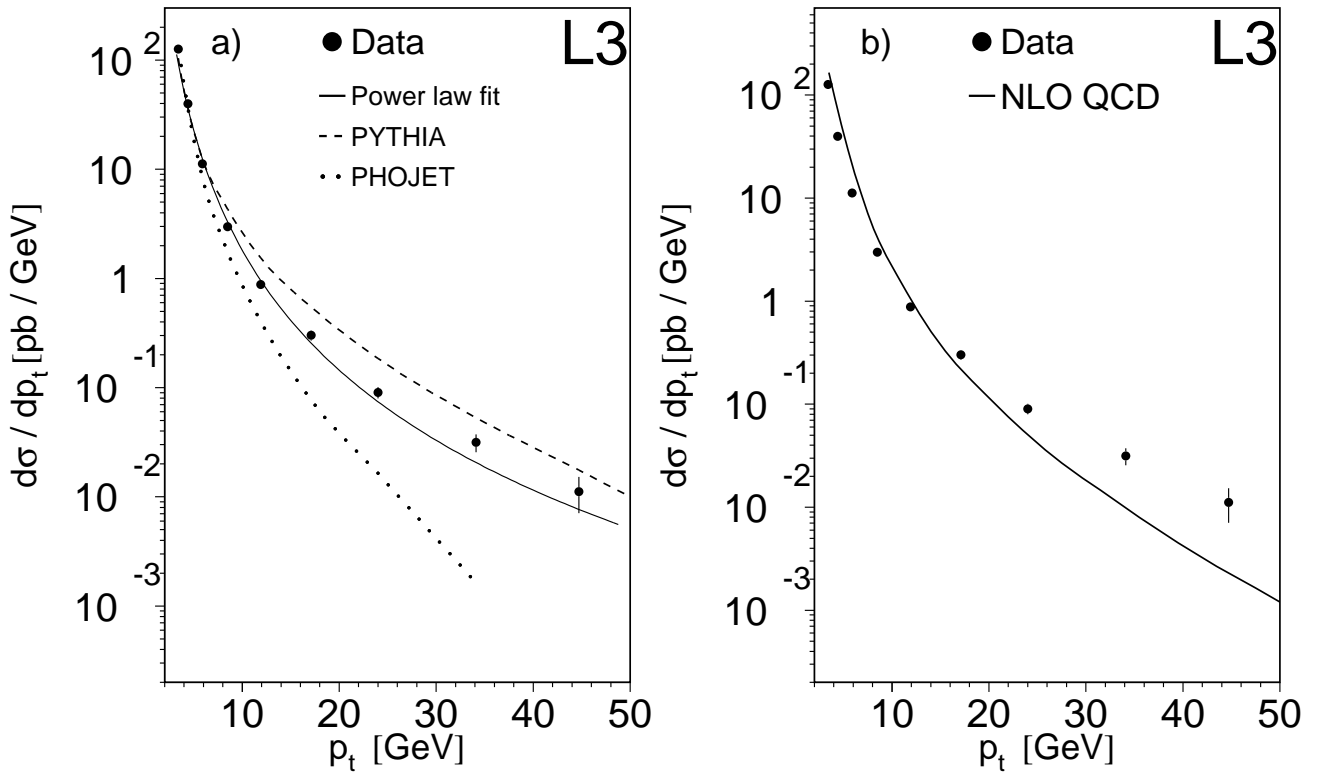
14

Figure 5: Inclusive jet differential cross section $d\sigma/dp_t$ a) compared to PYTHIA and PHOJET Monte Carlo predictions and the result of a power law fit (solid line); b) compared to NLO QCD calculations [2] (solid line). The theoretical scale uncertainty is less than 20%.
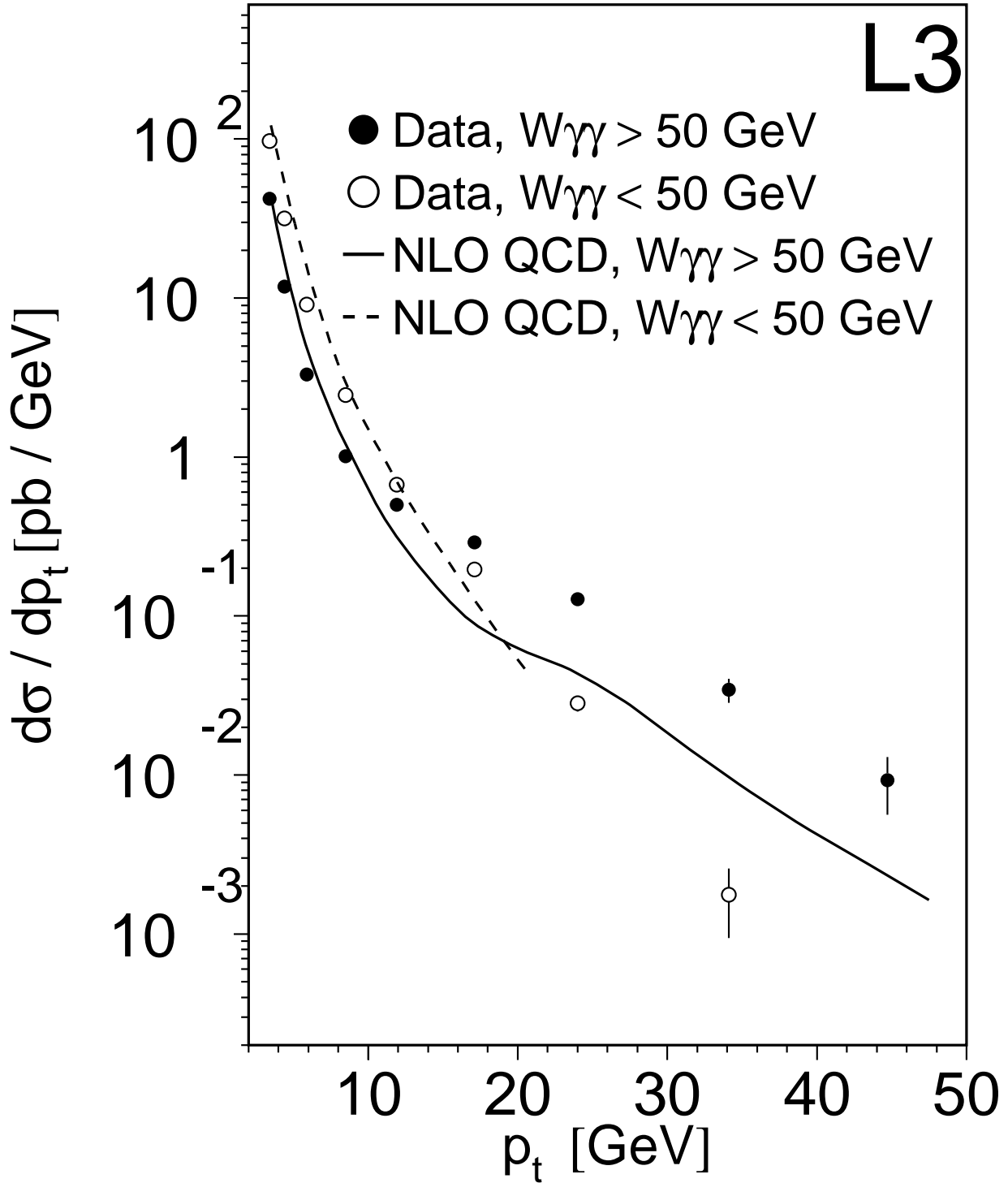
Figure 6: Inclusive jet differential cross section $d\sigma/dp_t$ for events with two-photon centre-of-mass energy, $W_{\gamma\gamma}$, below and above 50 GeV. NLO QCD calculations [2] are superimposed to the data. The discontinuity around 25 GeV is due to the direct contribution.